ULUSLARARASI 3B YAZICI TEKNOLOJİLERİ
VE DİJİTAL ENDÜSTRİ DERGİSİ

INTERNATIONAL JOURNAL OF 3D PRINTING TECHNOLOGIES AND DIGITAL INDUSTRY

ISSN:2602-3350 (Online)

URL: https://dergipark.org.tr/ij3dptdi

EVALUATION OF MECHANOBIOLOGICAL POTENTIAL OF 3D-PRINTED PLA BONE TISSUE SCAFFOLDS WITH DIFFERENT PORE ARCHITECTURES AND POROSITY RATIOS

Yazarlar (Authors): Safa ŞENAYSOY*, Hüseyin LEKESİZ

Bu makaleye şu şekilde atıfta bulunabilirsiniz (To cite to this article): *Şenaysoy S., Lekesiz H., "Evaluation of Mechanobiological Potential of 3D-Printed PLA Bone Tissue Scaffolds With Different Pore Architectures and Porosity Ratios" Int. J. of 3D Printing Tech. Dig. Ind., 8(2): 173-184, (2024).*

DOI: 10.46519/ij3dptdi.1449545

Araştırma Makale/ Research Article

Erişim Linki: (To link to this article): https://dergipark.org.tr/en/pub/ij3dptdi/archive

EVALUATION OF MECHANOBIOLOGICAL POTENTIAL OF 3D-PRINTED PLA BONE TISSUE SCAFFOLDS WITH DIFFERENT PORE ARCHITECTURES AND POROSITY RATIOS

Safa ŞENAYSOY[a]*, Hüseyin LEKESİZ[a]

[a]Bursa Technical University, Engineering and Nature Science Faculty, Mechanical Engineering Department, TÜRKİYE

* *Corresponding* safa.senaysoy@btu.edu.tr

(**Received:** 09.03.2024; **Revised:** 17.06.2024; **Accepted:** 12.08.2024)

ABSTRACT

Lattice structures are widely used in bone tissue scaffold designs due to interconnected porous structures that mimic the natural extracellular matrix (ECM) to treat large bone defects. This study investigated the mechanical behavior of scaffolds with different pore architectures and porosity ratios using experimental and numerical methods. In addition, mechanobiological potentials of scaffolds were evaluated in terms of the specific energy absorption and the specific surface area. Three different geometries were created by varying the combination of vertical, horizontal, and diagonal struts to evaluate the geometric factor and 50%, 62.5, and 75% porosity ratios are examined as potential permeabilities. Compression tests were performed to calculate stiffness values and energy absorptions of the scaffolds. Finite element simulations were used to obtain stiffness values of scaffolds. The specific energy absorptions of scaffolds were calculated under 4 N compressive load as a representative of potential body loads. According to the results, it was found that pore architectures and porosity ratios had crucial effects on stiffness values, energy absorption levels, specific energy absorption, and specific surface area which may lead to significant differences in bone remodeling. The highest specific energy absorption was observed in the scaffolds designed with only diagonal struts with 75% porosity. The highest specific surface area was observed in the scaffolds designed with the combination of vertical, horizontal, and diagonal struts with 75% porosity.

Keywords: Bone Tissue Scaffold, Mechanical Behavior, Mechanobiology, Bone Regeneration, Finite Element Analysis, Polylactic Acid (PLA)

1. INTRODUCTION

Bone tissue undergoes continuous remodeling processes that regulate bone formation and resorption throughout life [1-4]. The remodeling process allows bone tissue to regenerate, repair microdamage, and adapt to external mechanical loads [5-8]. Large defects in bone tissue can be caused by severe trauma or cancer, and they cannot be healed by remaining bone tissue. There are therapeutic methods to treat large bone defects, such as autograft, allograft, and xenograft. Nevertheless, these methods have some limitations in surgical operations due to insufficient tissue, the lack of donors, and immunity problems [9-12]. Tissue engineering has emerged as a promising alternative to traditional approaches for treating large bone defects [13-16, 20]. The tissue engineering approach uses different components such as cultured cells, scaffolds, and growth factors to facilitate tissue regeneration [17]. Bone tissue scaffolds replace extracellular matrix (ECM) that stimulates bone regeneration by mimicking the native tissue [18-19]. Since bone tissue scaffold plays a crucial role in bone tissue engineering, it should possess the following properties: porous structures to allow bone cell growth, vascularization, and diffusion of nutrients; mechanical strength to carry external loads during the bone-forming process; biocompatibility and biodegradation [20-24]. Moreover, bone remodeling is a mechanobiological phenomenon that can be affected by mechanical stimulation [1, 25-28]. Therefore, mechanical stimulation on scaffold

has an important effect on bone regeneration, and it can be adjusted by changing pore architecture and porosity ratio. Studies have demonstrated that pore architectures in scaffolds significantly determine mechanical properties, including strength, stiffness, and energy absorption [29-31]. In addition, the porosity ratio in the scaffold has essential effects on mechanical behavior, surface area, and interconnectivity, which are vital for bone regeneration [32]. In a study by Dawson et al., it was reported that the rate of bone tissue regeneration may increase with increasing scaffold porosity [33]. On the other hand, Buizer et al. explained that scaffolds with a high porosity ratio can show higher bone tissue ingrowth than scaffolds with a lower porosity ratio [34]. The reason is that the specific surface area of scaffolds increases with the porosity ratio and affects cell adhesion, growth, and nutrient-oxygen transportation.

The additive manufacturing technique, which has seen significant improvements in the last few decades, plays a pivotal role in scaffold production by allowing the creation of scaffolds with the desired pore architecture and porosity [35]. Lattice structures are well-known structures especially used in scaffold production which brings the advantage of controllability of manufacturing with Fused Deposition Modeling (FDM). The ability to create different pore architectures and porosity ratios in bone tissue scaffolds leads to different mechanical stimulation levels. As a result, the bone regeneration process can be controlled by changing pore architectures and porosity ratios with the help of flexible additive manufacturing methods. Polymers, particularly popular biomaterials used in tissue engineering, have many attractive properties, such as biocompatibility and biodegradability [36]. One of the most popular biomaterials used in bone tissue scaffolds is polylactic acid (PLA) due to its compressive strength and its high compatibility with additive manufacturing [37].

This study adopts a comprehensive approach to determine the mechanical behavior of bone tissue scaffolds with different pore architectures and porosity ratios. Three different pore architectures, Basic Cube (BC), Body-Centered Structure (BCS), and Body-Centered Cubic (BCC), were selected, and their designs were adjusted to achieve 50%, 62.5%, and 75% porosity ratios. The mechanical behavior of the scaffolds was determined using a combination of experimental and numerical methods. The experimental methods involved compressive tests, while the finite element method was used to predict the behavior of the scaffolds in the linear-elastic region. The mechanical properties of the scaffolds were also evaluated in terms of the specific energy absorption and the specific surface area under a 4 N load, forming the desired stress levels on the bone tissue scaffolds.

2. MATERIALS AND METHODS

2.1. Design and Printing of Bone Tissue Scaffolds

Three pore architectures and porosity ratios were chosen to design bone tissue scaffolds. These pore architectures were named Basic Cube (BC), Body-Centered Structure (BCS), and Body-Centered Cubic (BCC). The design of scaffolds, voxel meshed scaffolds, and 3D-printed scaffolds are illustrated in Figure 1.

The main reason for choosing these three designs is to create various combinations of axial and bending loadings so that the influence of different stresses can be investigated in detail. BC scaffolds present only struts in vertical and horizontal directions with major axial stress distribution. BCS scaffolds grant all bending loading with no axial support. On the other hand, the joints of all struts create a large surface area for bone cells to attach. BCC scaffolds combine axial and bending elements and therefore arise both stress types.

The well-known advantage of these three structures is that three-region (linear, plateau, and densification) force-displacement behavior can easily be controlled as suggested by Gibson [38]. However inconceivable disadvantages such as intense joint area along with possible printing deficiencies also need to be examined carefully. An auxiliary factor for choosing these specific lattice designs is that porosity can be assigned easily by changing basic parameters such as the length and cross-section of struts. The design parameters of the unit scaffold are shown in Figure 1a, and each unit scaffold was designed for 50%, 62.5%, and 75% porosity ratios. The naming of scaffolds is derived from combination their pore architectures and porosity ratios and is given in Table 1.

The unit scaffolds were patterned twice in the x, y, and z directions, and the periodic scaffolds were obtained. In addition, the specific surface

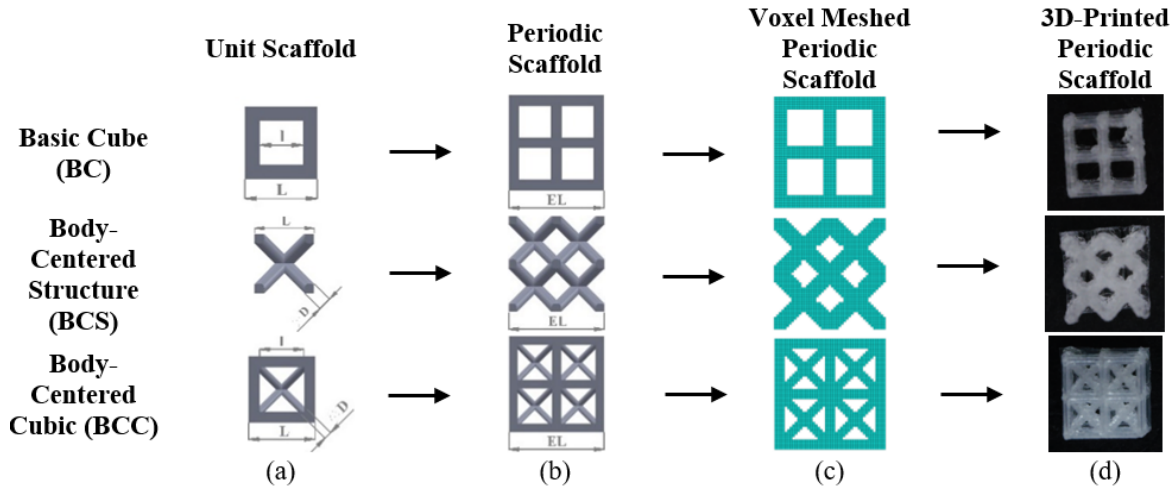

Figure 1. The Design of Scaffolds, Voxel Meshed Scaffolds, and 3D-Printed Images (a) Design of Unit Scaffolds (b) Design of Periodic Scaffolds (c) Voxel Meshed Scaffolds (d) 3D-Printed Scaffolds

Table 1. Design Parameters and Properties of Scaffolds

Scaffold	Length of Periodic Scaffold Edge (mm)	Length of Unit Scaffold Edge (L mm)	Length of Unit Scaffold Porous Edge (l mm)	Diameter of Rod (D mm)	Porosity Ratio (%)	Surface Area (mm^2)	Volume (mm^3)	Specific Surface Area (mm^{-1})	Mass (mg)
BC50	5.400	3	1.290	-	50.220	275.023	67.800	4.056	86.925
BC62.5	5.270	3	1.540	-	62.550	271.604	54.820	4.954	70.575
BC75	5.145	3	1.800	-	74.080	252.720	40.820	6.191	56.125
BCS50	5.390	3	-	1.000	51.640	254.724	75.430	3.377	94.600
BCS62.5	5.470	3	-	0.860	62.500	250.681	61.380	4.084	79.025
BCS75	5.580	3	-	0.690	74.630	233.096	44.070	5.289	54.475
BCC50	5.500	3	2.000	0.880	49.960	374.585	83.250	4.500	105.800
BCC62.5	5.500	3	2.000	0.660	62.450	369.320	62.470	5.912	75.900
BCC75	5.500	3	2.000	0.350	75.840	326.319	40.200	8.117	55.275

area of scaffolds was determined by dividing the surface area by volume. The design variables and properties of scaffolds are given in Table 1.

Table 2. Printing Parameters

Parameter	Value
Nozzle Temperature	200 ^{0}C
Nozzle Diameter	0.25 mm
Build Plate Temperature	60 ^{0}C
Printing Speed	30 mm/s
Layer Thickness	0.1 mm
Infill Density	100%

The designed periodic scaffolds were printed with Ultimaker 3 Extended 3D printer based on fused deposition modeling (FDM). Polylactic-acid (PLA) filament with 2.85 mm diameter was utilized to print periodic scaffolds. Printing parameters are given in Table 2.

PLA is approved by Food and Drug Administration (FDA) as biomaterial and therefore printing parameters are already well-characterized thank to its wide range of use. All scaffold geometries and all porosities are produced using the same parameters to avoid unexpected factors affecting consistency. Printing parameters such as infill, nozzle diameter, and temperature may also influence mechanical properties, therefore stable production is critical for proper evaluation of differences between designs, and this was made possible with the parameters given in Table 2.

2.2. Mechanical Behavior of Periodic Scaffolds

The mechanical behavior of periodic scaffolds with different pore architectures and porosity ratios were determined by compression test. Compression tests were performed using a universal test machine (Shimadzu AGS-X) at Bursa Technical University Mechanical Testing Laboratory. The universal test machine has 1 kN maximum load capacity. Compression test speed was selected as 0.3 mm/min. Compression tests were carried out up to 2.5 mm displacement for each scaffold, and force-displacement data was recorded using Trapezium X software. Stiffness values were calculated from the slope of the linear region of force-displacement curves for each scaffold. The total energy absorption value (E_T) for each scaffold was determined from the area under the force-displacement curve using Equation 1.

$$E_T = \int_0^{\delta} F d\delta \quad (1)$$

where δ is displacement and F is compression force. Moreover, each scaffold's specific energy absorption (SEA) value was calculated using Equation 2 [39].

$$SEA = {E_T}/{m} \quad (2)$$

where E_T is the total energy absorption and m is the mass of the scaffold. The mass of the scaffolds was measured by Radwag 220∓ 0.0001g analytical balance.

2.3. Finite Element Analysis of Periodic Scaffolds

Finite element analyses were performed on periodic scaffolds to obtain stiffness values, von mises stress, and equivalent strain distributions. The structure is meshed similar to voxel meshing with a length of 125 µm for all scaffolds. Each voxel mesh element had linear 8-node brick element properties [40]. Voxel meshed periodic scaffolds with three different pore architectures for 75% porosity ratio are given in Figure 1c. As boundary conditions, the bottom side of the scaffolds were fixed, and nodal displacement was applied perpendicular to the upper side of the scaffolds. The boundary conditions of scaffolds are illustrated in Figure 2.

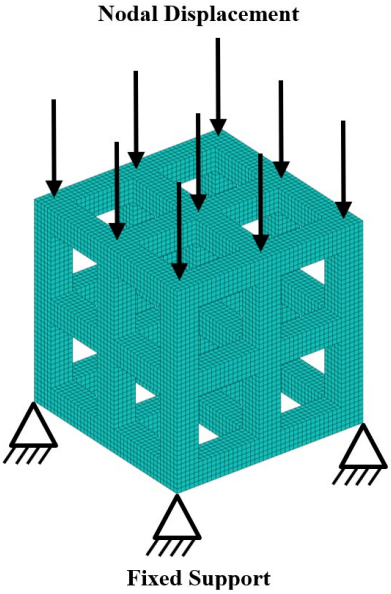

Figure 2. Boundary Conditions of Finite Element Analysis for Scaffold

The material properties of scaffolds were assumed to exhibit linear-elastic behavior in the finite element analysis. Young's modulus of scaffold material is taken as 1350 MPa. The porous nature and imperfections in structures due to FDM procedure are adjusted by equating experimental stiffness in linear region to stiffness obtained from FEM analysis of basic cube with 75%. This scaffold is chosen due to its high potential as the most robust scaffold. Elastic modulus obtained from this justification yields a good match for other geometries (Basic Cube and Body-Centered Cubic) and other porosities (50% and 62.5%).

Poisson's ratio of scaffold material was assumed to be 0.3 in the finite element analysis. The stiffness values of scaffolds were calculated from the slope of force-displacement curves obtained from linear finite element analysis. To obtain von Mises stress and equivalent strain distributions of scaffolds, 4 N load, which creates 1-2 MPa stress on scaffolds, was selected in the finite element analysis since 1-2 MPa stress in scaffolds is the desired stress level [41].
Post-yielding (plasticity and damage) behavior of the material is not considered in the analysis because excessive deformation is not acceptable for scaffolds. As mentioned previously, the stress level for optimum bone growth is significantly less than yielding stress. Furthermore, newly formed bone shares stress and stress decreases as the bone remodeling process continues, therefore, plasticity and damage are not involved in the process.

All linear-elastic finite element implementations are done using custom MATLAB coding written by authors.

3. RESULTS AND DISCUSSIONS

3.1. Stiffness Values of Periodic Scaffolds

The stiffness values obtained from the compression test and finite element analysis are given in Figure 3. As the porosity ratio of scaffolds increases, their stiffness values start to decrease in both compression tests and finite element analysis results. BC scaffold had the highest stiffness values for all porosity ratios since it consisted of thick vertical and horizontal struts rather than BCS and BCC scaffolds. Although the BCC scaffold had vertical and horizontal struts in addition to diagonal struts, the BCC scaffold's vertical and horizontal struts were thinner than the BC scaffold. Therefore, the BCC scaffolds had the second-highest stiffness values for all porosity, except in the finite element analysis, where 50% porosity ratio was observed. The BCS scaffolds had the lowest stiffness values for all porosity ratios in experimental results.

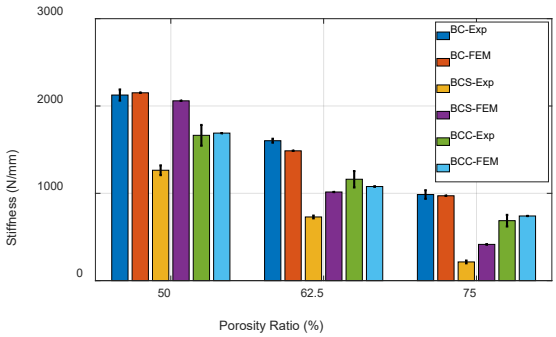

Figure 3. Stiffness Values of Periodic Scaffolds

When the experimental and finite element analysis results are compared, it is seen that they are close to each other except for the BCS results. BCS geometry involves only diagonal struts, and this leads mostly to bending loading which forces joints to rotate while joints are mostly modeled as fixed support in analytical models [38]. The length of the struts is also smaller, and this makes transverse shear comparable with flexural stress as in short beams. Furthermore, joints have the highest volume because the number of struts meeting at a common joint is also the highest. This leads to multiple concave surfaces around the joint and these surfaces may not be printed as modeled on the FE model. Therefore, a smooth joint with fixed support characteristics is not a valid assumption for these structures. On the other hand, transverse shear cannot be captured well in FEA. The mismatch can be attributed to these factors; however, printing deficiencies may also influence this mismatch. As indicated in the previous section, scaffolds were printed using fused deposition modeling (FDM). Printing parameters may affect the mechanical properties of scaffolds used in bone tissue engineering. Dimensional precision and accuracy in 3D printing are crucial for fabricating scaffolds with the desired mechanical properties. In addition, the 3D printing process can contain imperfections in the printed scaffolds, which can significantly affect the mechanical properties of scaffolds. These imperfections may be irregularities in the

printed layers, differences in material deposition, or incomplete fusion between layers, leading to variations from the desired pore geometry and mechanical properties of scaffolds, affecting their performance in bone tissue engineering. Differences between the experimental and finite element analysis results in BCS scaffolds may be related to the printing imperfections since BCS scaffolds consist of only diagonal struts, and printing diagonal struts are more complex than vertical struts.

3.2. Stress and Strain Distributions of Periodic Scaffolds

In bone tissue engineering applications, scaffolds are required to remain in the linear region under mechanical stimulation, and the desired stress levels on scaffolds under mechanical stimulation are approximately 1-2 MPa. Von Mises stress and equivalent strain distribution of scaffolds obtained from finite element analysis are illustrated in Figure 4. It was found that as the porosity of the scaffolds increased, the von Mises stress and equivalent strain values increased. The BCS75 scaffold

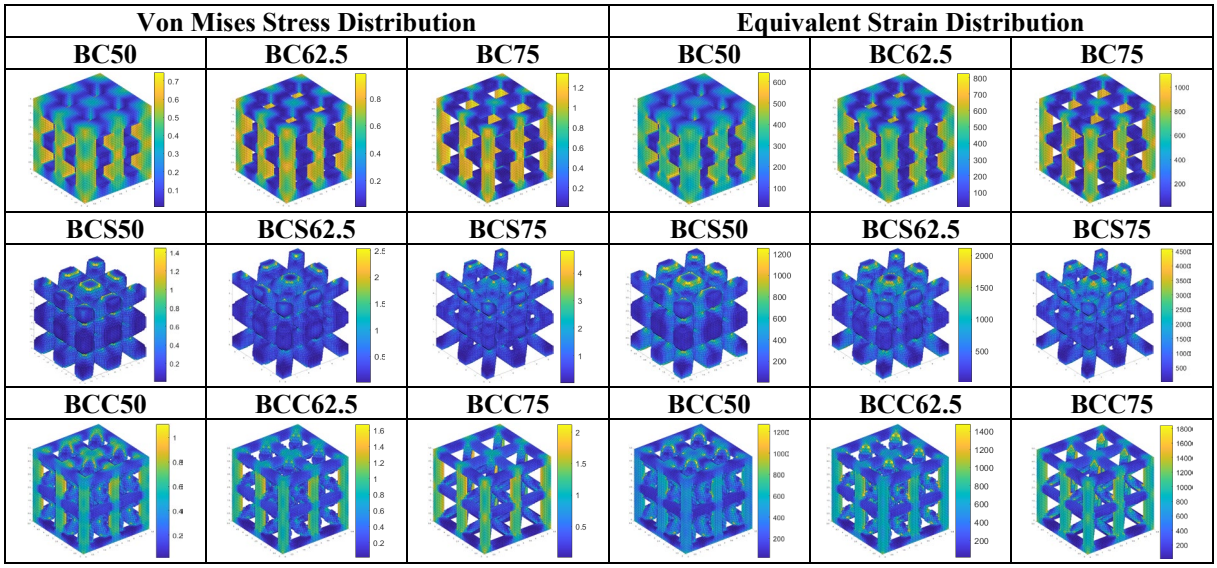

Figure 4. Von Mises Stress and Equivalent Strain Distributions for Scaffolds under 4 N Load

had the highest Von Mises stress and equivalent strain values. When Von Mises stress and equivalent strain values of scaffolds were compared with each other at the same porosity ratio, the BCS scaffolds had the highest values. The BCC scaffolds had the second-highest values, and the BC scaffolds had the lowest values. These results were consistent with the stiffness values of scaffolds. However, Von Mises' stress and equivalent strain values of the BCS75 scaffolds under 4 N load were approximately twice higher than those of other scaffolds. In bone tissue engineering applications, it should be taken into consideration that BCS75 scaffolds may fail due to their high Von Mises stress and equivalent strain values compared to other scaffolds.

3.3. Mechanical Behavior of Periodic Scaffolds under Compression Loading

Scaffolds under compression loading exhibit three different regions. These are elastic, plateau, and densification regions. Plateau region happens because of post-yielding behavior of PLA and densification occurs as a result of the failure of PLA. These three regions typically indicate the porous and cellular structure of scaffolds [38]. In the elastic region, struts of scaffolds exhibit linear behavior. After the elastic limits of scaffolds are exceeded, the plateau region starts. In this region, scaffold struts can exhibit elastoplastic or brittle behavior depending on the scaffold material [38]. Moreover, if the struts of scaffolds are slender enough, buckling in scaffold struts can be observed. Therefore, the force in the plateau region almost stays constant while displacement is increasing. After the plateau region, the scaffolds start to collapse in the densification region, and the struts of the scaffolds stack up

with each other [38]. Therefore, the force starts to increase. These regions have a crucial effect on the energy absorption behavior of scaffolds. The force-displacement behavior and the energy absorption behavior of periodic scaffolds obtained from compression tests are shown in Figure 5.

For scaffolds with 50% porosity, elastic and densification regions were more prominent up to 2.5 mm displacement while there was a gradual increase in stiffness between elastic and densification regions. Thick struts in 50% BCS create stacked and stiffer joints and therefore structure experiences a hardening as compression is sustained. This results in a shorter plateau region. On the contrary, slender struts in 75% porous scaffolds create more flexible joints and more chance of collapsing by buckling which means an extended plateau region.

For scaffolds with 62.5% porosity ratio, BCS scaffold reached the densification region first, therefore BCS62.5 scaffold had the highest force value at 2.5 mm displacement. By recalling that BCS involves only diagonal struts behaving mostly as beams, a possible explanation for this phenomenon is that short beams for 62.5% lead dominantly to shear loading and therefore fail prematurely. Beams

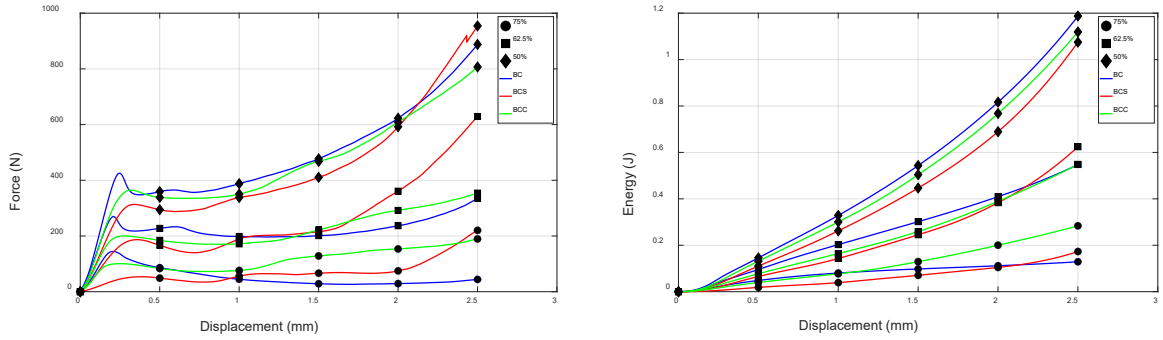

a) **b)**

Figure 5. Compression Test Results of Periodic Scaffolds **a)** Force-Displacement Graphics **b)** Energy-Displacement Graphic

are even shorter for 50% porous scaffolds; however, joint stiffness is also higher as explained in the previous paragraph and therefore, strut failure is less likely.

For 75%-porous scaffolds, only BCS75 reached the densification region, while BC75 scaffold remained in the plateau region. Therefore, BC75 scaffold had the lowest force value at 2.5 mm displacement.

When the energy absorption behavior of scaffolds in Figure 5b were examined, it was observed that as the porosity of the scaffolds increases, the amount of energy absorption also increases. In 50% porosity ratio, it was seen that the BC scaffold had the highest energy absorption amount at the end of 2.5 mm displacement. The BCC scaffold had the second-highest energy absorption amount, and the BCS scaffold had the lowest energy absorption amount. These results were proportional to the stiffness results of scaffolds. In the 62.5% porosity ratio, the energy absorption was proportional to the stiffness values of scaffolds up to 2 mm displacement. However, the BCS scaffold exhibited the highest energy absorption at 2.5 mm displacement. This changing behavior may be attributed to the compression behavior of scaffolds. The BCS62.5 scaffolds reached the densification region after 2 mm displacement, while the BC62.5 and BCC62.5 scaffolds were still in the plateau region. In the 75% porosity ratio, although the energy absorption amounts were proportional to the stiffness values of scaffolds up to 1 mm, the energy absorption behavior changed after 1 mm displacement. Finally, the BCC75 scaffolds had the highest energy absorption at 2.5 mm displacement. The BC75 scaffolds had the highest stiffness among 75% porosity scaffolds but it has the lowest energy absorption amount at the 2.5 mm displacement. Since the struts of BC scaffolds were slenderer than those of BCS and BCC scaffolds, they underwent buckling damage in the plateau region. Therefore, it couldn't carry

the load and had the lowest energy absorption amount at 2.5 mm displacement.

3.4. Evaluation of Mechanobiological Potentials of Periodic Scaffolds

The mechanical properties of bone tissue scaffolds play a crucial role in bone tissue regeneration. Since the bone regeneration process is a mechanobiological phenomenon, the strain energy distribution, especially on the bone tissue scaffold, critically impacts long-term bone regeneration [1-4, 43]. Therefore, different strain energy distributions in bone tissue scaffolds can lead to the formation of heterogeneous bone density [44]. In this study, the effect of strain energy on bone regeneration behavior in bone tissue scaffolds was evaluated by using compression test data up to 4 N loading for bone tissue scaffolds. The specific energy absorption was determined by dividing the total strain energy obtained up to 4 N loading by the mass of the scaffold. The specific energy absorption may be assumed as mechanical stimulation in the bone regeneration process, and higher mechanical stimulation on bone tissue scaffold may lead to higher bone regeneration. Therefore, the specific energy absorption amount is one of the vital mechanical properties in designing bone tissue scaffolds [44]. Furthermore, the specific surface area of bone tissue scaffolds is one of the important factors in bone tissue engineering since it affects bone tissue regeneration processes [45].

Cell adhesion, infiltration, and proliferation on 3-D scaffolds are already confusing topics that have not been investigated comprehensively in the literature. Therefore, geometry and mechanics relation to cell behavior is not clear yet. The continuum of this work will solely focus on these issues. On the other hand, it is already well known that bone cells are highly sensitive to mechanical stimulation via receptors in osteocyte-type cells. This sensitivity mostly results in complex procedures of bone regeneration which includes both formation and resorption. Based on preliminary work on in-vitro 3-D bone scaffolds, cells are sympathetic to both mechanical stimulation and largely curved surfaces [45].

The results of the specific energy absorption and the specific surface area for bone tissue scaffolds are depicted in Figure 6. According to the figure, the results of specific energy absorption were generally proportional to the stiffness values of bone tissue scaffolds, i.e., the stiffest structure BC50 has the lowest specific energy while the softest structure BCS75 has the highest specific energy. This is the result of the high deformation capacity of the overall scaffold rather than individual strut deformations. In other words, struts remain in the linear elastic region without reaching the yielding point even for higher overall deformations. This can be attributed to the fact that joints experience less resistance, and this leads joints to behave more like a pin joint rather than a fixed support resulting in a larger joint rotation. Larger rotation of joints means larger overall deformation without struts to reach yielding stress.

For scaffolds with the same pore architecture, the specific energy absorption of all scaffolds decreased as the porosity ratio increased. The BCS75 scaffold had the highest specific energy absorption amount under 4 N loading since it had the lowest stiffness value.

On the other hand, the BC50 scaffold had the lowest specific energy absorption since it had the highest stiffness value. When the specific surface areas of bone tissue scaffolds were examined, it was determined that the pore architecture of scaffolds had a significant effect on the specific surface area.

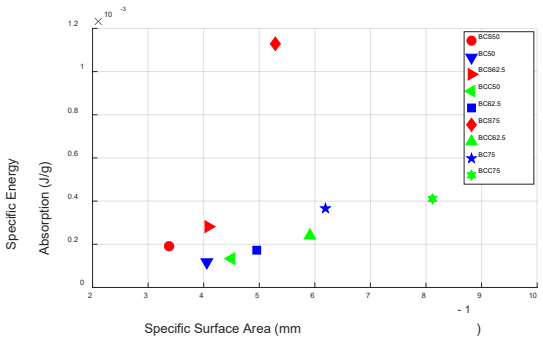

Figure 6. Specific Energy Absorption – Specific Surface Area Graph for Bone Tissue Scaffolds

Moreover, the specific surface area of all scaffolds increased as the porosity ratio increased in scaffolds with the same pore architecture. The highest specific surface area was observed in the BCC75 scaffold. However, the lowest specific surface area was found in the BCS50 scaffold. This means one can create more surface area for bone cells to attach for

BCC75 using less material and this creates efficiency while one needs to use more material to create surface area for BCS50 which is inefficient. However, surface area is not the only factor influencing cell growth and mechanical stimulation is also an important factor where specific energy becomes more critical.

Optimization algorithms can be utilized based on results produced in this work to evaluate how to change parameters for better bone remodeling. However, bone remodeling on 3-D scaffolds still requires extensive research to identify the procedure in detail. At first glance, a scaffold combining stimulation with the high specific surface area would lead to optimum design and therefore, some design between BCC 75 and BCS 75 seems the best option. This may be possible by joining diagonal struts in the middle of the adjacent strut rather than all at the center of the cube. However, these types of structures are projected to lead to several manufacturing issues.

4. CONCLUSION

This study aimed to evaluate the usage of scaffolds with different pore architectures and porosity ratios in bone tissue engineering in terms of mechanical properties using the compression test and finite element analysis. Basic Cube (BC), Body-Centered Structure (BCS), and Body-Centered Cubic (BCC) were chosen as pore architectures for bone tissue scaffolds. The porosity ratios of scaffolds were adjusted by changing the design parameters of the scaffolds. The stiffness values, energy absorption behaviors, and specific energy absorptions for bone tissue scaffolds were obtained from compression tests. The specific energy absorption was calculated under 4 N compressive loading, forming the desired stress level on the scaffold. The Von Mises stress, and equivalent strain distributions on scaffolds under 4 N loading were obtained from finite element analysis. Moreover, the stiffness values of scaffolds were calculated from finite element analysis. The compression test and finite element analysis results for scaffolds are summarized below.

- As the porosity ratios of all scaffolds increased, the stiffness values decreased in both experimental and finite element results.
- BC50 scaffold had the highest stiffness value since it had thicker vertical and horizontal struts than the other scaffolds. BCS75 scaffold had the lowest stiffness value since it only consisted of diagonal struts.
- The results of stiffness values obtained from the compression test and finite element analysis were found to be consistent with each other except for BCS scaffolds. Since the printing processes of diagonal struts were more complex than vertical and horizontal struts, these inconsistent results of BCS scaffolds may be related to the printing imperfections. As the printing imperfections have an essential effect on the stiffness values of scaffolds, they should be considered in the design and printing of scaffolds.
- The maximum Von Mises stress, and equivalent strain levels of the BCS75 scaffold were almost twice that of the other scaffolds. Therefore, BCS75 scaffolds may fail in usage.
- The energy absorption level increased as the porosity ratio decreased. BC50 scaffold had the highest energy absorption level, while the BC75 scaffold had the lowest. The energy absorption levels were proportional to the stiffness values of scaffolds at the 50% porosity ratio. However, the plateau region's behavior started to dominate the scaffolds' energy absorption levels at the 62.5% and 75% porosity ratios.
- BCS75 scaffold had the highest specific energy absorption level, while the lowest specific energy absorption level was observed in the BC50 scaffold. The specific energy absorption level increased as the porosity ratio increased in scaffolds with the same pore architecture.
- BCC75 scaffold had the highest specific surface area, while the lowest specific surface area was found in the BCS50 scaffold. It was determined that the specific surface area increased as the porosity ratio of scaffolds with the same pore architecture increased. It was also observed that pore architecture significantly impacted the specific surface area.

The specific energy absorption and surface area are essential properties of bone tissue scaffolds. BCS75 scaffold had the highest specific energy

absorption, while BCC75 scaffold had the highest specific surface area and the second highest specific energy absorption. Therefore, it is considered advantageous to use the BCC75 scaffold in bone tissue engineering.

ACKNOWLEDGMENTS

This study was supported by the Scientific and Technological Research Council of Turkey (TUBITAK) (Project No. 222M025)

REFERENCES

1. Li, J., Li, H., Shi, L., Fok, A. S., Ucer, C., Devlin, H., ... & Silikas, N., "A mathematical model for simulating the bone remodeling process under mechanical stimulus", Dental materials Vol. 13, Issue 9, Pages 1073-1078, 2007.

2. Zhao, Y., & Zhang, G., "A computational study of the dual effect of intermittent and continuous administration of parathyroid hormone on bone remodeling", Acta Biomaterialia, Vol. 93, Pages 200-209, 2019.

3. Cowin, S. C., & Hegedus, D., "Bone remodeling I: theory of adaptive elasticity", Journal of Elasticity, Vol. 6, Pages 313-326, 1976.

4. Pearce, C. J., "Efficient numerical analysis of bone remodelling", Journal of the Mechanical Behavior of Biomedical Materials, Vol. 4, Issue 6, Pages 858-867, 2011.

5. Zhang, Y., Zhang, C., Wang, J., Liu, H., & Wang, M., "Bone-Adipose Tissue Crosstalk: Role of Adipose Tissue Derived Extracellular Vesicles in Bone Diseases", Journal of Cellular Physiology, Vol. 236, Issue 11, Pages 7874-7886, 2021.

6. Shoji-Matsunaga, A., Ono, T., Hayashi, M., Takayanagi, H., Moriyama, K., & Nakashima, T., "Osteocyte regulation of orthodontic force-mediated tooth movement via RANKL expression", Scientific reports, Vol. 7 Issue 1, 8753, 2017.

7. Rémond, A., Naïli, S., & Lemaire, T., "Interstitial fluid flow in the osteon with spatial gradients of mechanical properties: a finite element study", Biomechanics and modeling in Mechanobiology, Vol. 7, Pages 487-495, 2008.

8. Smit, T. H., & Burger, E. H., "Is BMU-coupling a strain-regulated phenomenon? A finite element analysis", Journal of Bone and Mineral Research, Vol. 15, Issue 2, Pages 301-307, 2000.

9. Nwankwo, E. C., Chen, F., Nettles, D. L., & Adams, S. B., "Five-year follow-up of distal tibia bone and foot and ankle trauma treated with a 3D-printed titanium cage", Case Reports in Orthopedics, Vol. 2019, 2019.

10. Fernandes, M. B. C., Guimarães, J. A. M., Casado, P. L., Cavalcanti, A. D. S., Gonçalves, N. N., Ambrósio, C. E., ... & Duarte, M. E. L., "The effect of bone allografts combined with bone marrow stromal cells on the healing of segmental bone defects in a sheep model", BMC veterinary research, Vol. 10, Issue 1, Pages 1-12, 2014.

11. Long, T., Zhu, Z., Awad, H. A., Schwarz, E. M., Hilton, M. J., & Dong, Y., "The effect of mesenchymal stem cell sheets on structural allograft healing of critical sized femoral defects in mice", Biomaterials, Vol. 35, Issue 9, Pages 2752-2759, 2014.

12. Zhao, Z. H., Ma, X. L., Zhao, B., Tian, P., Ma, J. X., Kang, J. Y., ... & Sun, L., "Naringin-inlaid silk fibroin/hydroxyapatite scaffold enhances human umbilical cord-derived mesenchymal stem cell-based bone regeneration", Cell Proliferation, Vol. 54, Issue 7, e13043, 2021.

13. Carulli, C., Matassi, F., Civinini, R., & Innocenti, M., "Tissue engineering applications in the management of bone loss", Clinical cases in mineral and bone metabolism, Vol. 10, Issue 1, Pages 22-25, 2013.

14. Guilak, F., Butler, D. L., Goldstein, S. A., & Baaijens, F. P., "Biomechanics and mechanobiology in functional tissue engineering", Journal of biomechanics, Vol. 47, Issue 9, Pages 1933-1940, 2014.

15. Mi, H. Y., Jing, X., & Turng, L. S., "Fabrication of porous synthetic polymer scaffolds for tissue engineering", Journal of Cellular Plastics, Vol. 51, Issue 2, Pages 165-196, 2015.

16. Paladini, F., & Pollini, M., "Novel approaches and biomaterials for bone tissue engineering: a focus on silk fibroin", Materials, Vol. 15, Issue 19, 6952, 2022.

17. Kagami, H., Agata, H., & Tojo, A., "Bone marrow stromal cells (bone marrow-derived multipotent mesenchymal stromal cells) for bone tissue engineering: basic science to clinical translation", The international journal of biochemistry & cell biology, Vol. 43, Issue 3, Pages 286-289, 2011.

18. Thein-Han, W. W., & Misra, R. D. K., "Three-dimensional chitosan-nanohydroxyapatite composite scaffolds for bone tissue engineering", JOM, Vol. 61, Pages 41-44, 2009.

19. Shadjou, N., & Hasanzadeh, M., "Graphene and its nanostructure derivatives for use in bone tissue engineering: Recent advances", Journal of Biomedical Materials Research Part A, Vol. 104, Issue 5, Pages 1250-1275, 2016.

20. Lin, C. Y., & Kang, J. H., "Mechanical properties of compact bone defined by the stress-strain curve measured using uniaxial tensile test: a concise review and practical guide", Materials, Vol. 14, Issue 15, 4224, 2021.

21. Chen, J., "Recent development of biomaterials combined with mesenchymal stem cells as a strategy in cartilage regeneration", International Journal of Translational Medicine, Vol. 2, Issue 3, Pages 456-481, 2022.

22. Qu, H., Fu, H., Han, Z., & Sun, Y., "Biomaterials for bone tissue engineering scaffolds: A review", RSC advances, Vol. 9, Issue 45, Pages 26252-26262, 2019.

23. Collins, M. N., Ren, G., Young, K., Pina, S., Reis, R. L., & Oliveira, J. M., "Scaffold fabrication technologies and structure/function properties in bone tissue engineering", Advanced functional materials, Vol. 31, Issue 21, 210609, 2021.

24. Suamte, L., Tirkey, A., Barman, J., & Babu, P. J., "Various manufacturing methods and ideal properties of scaffolds for tissue engineering applications", Smart Materials in Manufacturing, Vol. 1, 100011, 2023.

25. Wang, L., You, X., Zhang, L., Zhang, C., & Zou, W., "Mechanical regulation of bone remodeling", Bone Research, Vol. 10, Issue 1, 16, 2022.

26. Shi, Q., Chen, Q., Pugno, N., & Li, Z. Y., "Effect of rehabilitation exercise durations on the dynamic bone repair process by coupling polymer scaffold degradation and bone formation", Biomechanics and Modeling in Mechanobiology, Vol. 17, Pages 763-775, 2018.

27. Sun, W., Li, Y., Li, J., Tan, Y., Yuan, X., Meng, H., ... & Li, Y., "Mechanical stimulation controls osteoclast function through the regulation of Ca2+-activated Cl− channel Anoctamin 1", Communications Biology, Vol. 6, Issue 1, 407, 2023.

28. Vatsa, A., Mizuno, D., Smit, T. H., Schmidt, C. F., MacKintosh, F. C., & Klein-Nulend, J., "Bio imaging of intracellular NO production in single bone cells after mechanical stimulation", Bone and Mineral Research, Vol. 21, Issue 11, Pages 1722-1728, 2006.

29. Onal, E., Frith, J. E., Jurg, M., Wu, X., & Molotnikov, A., "Mechanical properties and in vitro behavior of additively manufactured and functionally graded Ti6Al4V porous scaffolds", Metals, Vol. 8, Issue 4, 200, 2018.

30. Deng, F., Liu, L., Li, Z., & Liu, J., "3D printed Ti6Al4V bone scaffolds with different pore structure effects on bone ingrowth", Journal of biological engineering, Vol. 15, Pages 1-13, 2021.

31. Karaman, D., & Ghahramanzadeh Asl, H., "Biomechanical behavior of diamond lattice scaffolds obtained by two different design approaches with similar porosity; a numerical investigation with FEM and CFD analysis", Proceedings of the Institution of Mechanical Engineers, Part H: Journal of Engineering in Medicine, Vol. 236, Issue 6, Pages 794-810, 2022.

32. Zhang, X. Y., Fang, G., Xing, L. L., Liu, W., & Zhou, J., "Effect of porosity variation strategy on the performance of functionally graded Ti-6Al-4V scaffolds for bone tissue engineering", Materials & Design, Vol. 157, Pages 523-538, 2018.

33. Dawson, E. R., Suzuki, R. K., Samano, M. A., & Murphy, M. B., "Increased internal porosity and surface area of hydroxyapatite accelerates healing and compensates for low bone marrow mesenchymal stem cell concentrations in critically-sized bone defects", Applied Sciences, Vol. 8, Issue 8, 1366, 2018.

34. Buizer, A. T., Veldhuizen, A. G., Bulstra, S. K., & Kuijer, R., "Static versus vacuum cell seeding on high and low porosity ceramic scaffolds", Journal of biomaterials applications, Vol. 29, Issue 1, Pages 3-13, 2014.

35. Kontogianni, G. I., Loukelis, K., Bonatti, A. F., Batoni, E., De Maria, C., Naseem, R., ... & Chatzinikolaidou, M., "Effect of Uniaxial Compression Frequency on Osteogenic Cell Responses in Dynamic 3D Cultures", Bioengineering, Vol. 10, Issue 5, 532, 2023.

36. Narayanan, G., Vernekar, V. N., Kuyinu, E. L., & Laurencin, C. T., "Poly (lactic acid)-based biomaterials for orthopaedic regenerative engineering", Advanced drug delivery reviews, Vol. 107, Pages 247-276, 2016.

37. Alavi, M. S., Memarpour, S., Pazhohan-Nezhad, H., Salimi Asl, A., Moghbeli, M., Shadmanfar, S., & Saburi, E., "Applications of poly (lactic acid) in bone tissue engineering: A review article", Artificial Organs, Vol. 47, Issue 9, Pages 1423-1430, 2023.

38. Gibson, L. J., "Cellular solids", Pages 93-172, Mrs Bulletin, Cambridge, 2003.

39. Demirci E., Şenaysoy S., Tuğcu S. E., "The Effect of Nozzle Diameter and Layer Thickness on Mechanical Behavior of 3D Printed PLA Lattice Structures Under Quasi-Static Loading", Int. J. of 3D Printing Tech. Dig. Ind., Vol. 7, Issue 1, Pages 105-113, 2023.

40. T. Chandrupatla and A. Belegundu, "Introduction to Finite Elements in Engineering", Pages 214-258, Cambridge University Press, Cambridge, 2022.

41. Gorriz, C., Ribeiro, F., Guedes, J. M., Folgado, J., & Fernandes, P. R., "A Biomechanical Approach for Bone Regeneration Inside Scaffolds Embedded with BMP-2", New Developments in Tissue Engineering and Regeneration, Vol. 51, Pages 67-86, 2019.

42. Li, J. J., Dunstan, C. R., Entezari, A., Li, Q., Steck, R., Saifzadeh, S., ... & Zreiqat, H., "A novel bone substitute with high bioactivity, strength, and porosity for repairing large and load-bearing bone defects", Advanced healthcare materials, Vol. 8, Issue 8, 1801298, 2019.

43. Milan, J. L., Planell, J. A., & Lacroix, D., "Simulation of bone tissue formation within a porous scaffold under dynamic compression", Biomechanics and modeling in mechanobiology, Vol. 9, Pages 583-596, 2010.

44. Shi, Q., Chen, Q., Pugno, N., & Li, Z. Y., "Effect of rehabilitation exercise durations on the dynamic bone repair process by coupling polymer scaffold degradation and bone formation", Biomechanics and Modeling in Mechanobiology, Vol. 17, Pages 763-775, 2018.

45. Tovar, N., Witek, L., Atria, P., Sobieraj, M., Bowers, M., Lopez, C. D., ... & Coelho, P. G., "Form and functional repair of long bone using 3D-printed bioactive scaffolds", Journal of tissue engineering and regenerative medicine, Vol. 12, Issue 9, Pages 1986-1999, 2018.